SNAREs, HOPS and regulatory lipids control the dynamics of vacuolar actin during homotypic fusion in *S. cerevisiae*

Surya Karunakaran*, Terry Sasser*, Sailasree Rajalekshmi and Rutilio A. Fratti‡

Department of Biochemistry, University of Illinois at Urbana-Champaign, 419 Roger Adams Laboratory, B-4, 600 S. Mathews Ave., Urbana, IL 61801, USA

*These authors contributed equally to this work
‡Author for correspondence (rfratti@illinois.edu)

Accepted 7 November 2011
Journal of Cell Science 125, 1683–1692

doi: 10.1242/jcs.091900

Summary

Homotypic vacuole fusion requires SNAREs, the Rab Ypt7p, the tethering complex HOPS, regulatory lipids and actin. In *Saccharomyces cerevisiae*, actin functions at two stages of vacuole fusion. Pre-existing actin filaments are depolymerized to allow docking and assembly of the vertex ring (a microdomain enriched in proteins and lipids that mediate fusion). Actin is then polymerized late in the pathway to aid fusion. Here, we report that the fusion machinery regulates the accumulation of actin at the vertex ring. Using Cy3-labeled yeast actin to track its dynamics, we found that its vertex enrichment was abolished when actin monomers were stabilized by latrunculin-B, independent of the extent of incorporation. By contrast, stabilization of filamentous actin with jasplakinolide markedly augmented actin vertex enrichment. Importantly, agents that inhibit SNAREs, Ypt7p and HOPS inhibited the vertex enrichment of actin, demonstrating that the cytoskeleton and the fusion machinery are interdependently regulated. Actin mobilization was also inhibited by ligating ergosterol and PtdIns(3)*P*, whereas the ligation or modification of PtdIns(4,5)P_2 augmented the vertex enrichment of actin. The proteins and lipids that regulated actin mobilization to the vertex did not affect the total incorporation of Cy3–actin, indicating that actin mobilization and polymerization activities can be dissociated during membrane fusion.

Key words: Fusion, Phosphoinositide, SNARE, HOPS, Phospholipase C, Actin dynamics

Introduction

Membrane trafficking is utilized by all eukaryotes for the transportation of cargo within cells, as well as for the import and export of cargo between the cell and its environment. These mechanisms of transport are mediated by a set of machinery that is conserved from yeast to metazoans (Jahn and Sudhof, 1999). Most transport pathways culminate in the fusion of donor and acceptor membranes and the transfer of cargo. In our studies we use vacuolar lysosomes purified from the yeast *Saccharomyces cerevisiae* to examine the regulation of homotypic vesicle fusion. Vacuole fusion requires the *N*-ethylmaleimide-sensitive factor attachment protein receptors (SNAREs) Vam3p, Vam7p, Vti1p and Nyv1p, the SNARE chaperones Sec18p (NSF) and Sec17p (α-SNAP), the Rab GTPase Ypt7p and its effector complex HOPS (homotypic fusion and vacuole protein sorting), and a set of regulatory lipids that includes ergosterol, diacylglycerol and phosphoinositides (Wickner, 2010). Vacuole fusion also requires actin and the remodeling of actin, which is regulated by Rho GTPases (Eitzen et al., 2002; Isgandarova et al., 2007).

Membrane fusion occurs through a series of regulated and experimentally separable stages. Each stage is controlled by a set of proteins and lipids that activate the machinery to drive fusion. During priming, inactive cis-SNARE complexes on individual membranes are disassembled through the function of Sec18p and Sec17p in an ATP-dependent manner (Mayer et al., 1996). Next, partner vacuoles are tethered together through the action of Ypt7p, HOPS and phosphatidylinositol 3-phosphate [PtdIns(3)*P*] (Boeddinghaus et al., 2002; Haas et al., 1995; Mayer and Wickner, 1997). The docking stage is characterized by the formation of trans-SNARE complexes that assemble between partner membranes (Ungermann et al., 1998), which stimulates the release of luminal Ca^{2+} (Merz and Wickner, 2004a). When vacuoles are drawn together during the tethering and docking stages, membranes become distorted and form three distinct morphological features. The boundary membrane is the area of contact between vacuoles that becomes tightly apposed and flattened. The vertex ring is the edge of the boundary membrane, where vacuoles make contact and become enriched with the proteins and lipids that drive fusion (Fratti et al., 2004; Wang et al., 2002; Wang et al., 2003). The outer edge is where vacuoles are not in contact with other membranes.

Actin controls a variety of cellular functions through its dynamics and state of polymerization. The formation of actin filaments (F-actin) is required for endocytosis, pinocytosis, phagocytosis, cytokinesis, cell motility and membrane fusion (Eitzen et al., 2002; Galletta et al., 2010; Pollard and Cooper, 2009; Pollard, 2010). Depending on the cellular function, the polymerization of actin deforms membranes into a variety of shapes including pseudopods, lamellipodia, filopodia, podosomes and pedestals (Albiges-Rizo et al., 2009; Hartwig and Yin, 1988; Mogilner and Keren, 2009; Vallance and Finlay, 2000). In most pathways, the regulation of actin polymerization has been linked

to lipids including PtdIns(4,5)P_2 and cholesterol, and more recently 3-phosphoinositides (Babst et al., 2000; Bohdanowicz et al., 2010; Rozelle et al., 2000). During vacuole fusion, actin remodeling occurs at two distinct stages of the pathway. Early in the fusion pathway, before trans-SNARE pairing, F-actin must depolymerize into globular actin (G-actin) monomers (Eitzen et al., 2002). Late in the pathway, G-actin polymerizes to drive the final stages of fusion, however, the mechanisms for this function remain unclear. There are multiple theories that link actin polymerization with the regulation of membrane fusion; one possibility is that the formation of actin fences trap membrane proteins into small domains (Tamkun et al., 2007). Therefore, it is possible that increasing the local concentration of SNAREs at the vertex through the function of actin fences would amplify and focus the force generated by trans-SNARE complex formation at the site of fusion. Another hypothesis is that F-actin generates energy that deforms membranes to facilitate fusion.

Here, we examined the role of the fusion machinery in regulating actin polymerization and vertex enrichment during vacuole fusion. Using fluorescent yeast actin to track the dynamics of actin pools during fusion we found that the vertex enrichment of actin was controlled by SNAREs, Ypt7p, HOPS, ergosterol and phosphoinositides.

Results

Actin dynamics on docked vacuoles

Actin remodeling is required for vesicle trafficking and vacuolar fusion. Although actin dynamics are required for the fusion machinery to operate, it is unclear whether the fusion machinery regulates actin polymerization or its vertex enrichment. It is also unclear whether the polymerization state of actin affects its accumulation at the vertex. Often, studies that monitored actin dynamics with fluorescence microscopy use fluorescently tagged DNase-I to label G-actin, phalloidin to label F-actin, or rabbit actin to incorporate into endogenous actin pools (Bubb et al., 2000; Eitzen et al., 2002; Wang et al., 2003). Here, we used purified Cy3-labeled yeast actin, which provides an advantage over the use of DNase-I, phalloidin or rabbit actin because yeast Cy3–actin can be used to monitor ongoing live actin dynamics without fixation, interference from a non-native probe or differences in affinities between actin homologs.

Actin is rapidly polymerized on vacuoles during fusion (Isgandarova et al., 2007). However, the relationship between vertex enrichment and polymerization had not been examined. Here, we tested whether vertex enrichment and polymerization were related. Using purified vacuoles from the *S. cerevisiae* strain DKY6281, we performed docking reactions in the presence of 15 nM Cy3-labeled yeast actin. To test the relationship between actin polymerization and its enrichment at the vertex, we used pharmacological agents to modulate the state of actin polymerization. Docking reactions were run for 30 minutes at 27℃ and treated with either latrunculin-B (LatB), to stabilize G-actin pools (Morton et al., 2000), or jasplakinolide (JP) to stabilize F-actin filaments and activate in vitro polymerization (Bubb et al., 2000). After incubation, vacuoles were stained with the lipophilic dye MDY-64, mixed with agarose and mounted onto glass slides for observation by fluorescence microscopy. We found that Cy3–actin formed puncta that localized to the vertices of docked vacuoles and not at the boundary membrane or outer edges of the vesicles (Fig. 1A–C). Treatment with LatB blocked the vertex enrichment of Cy3–actin (Fig. 1D–F),

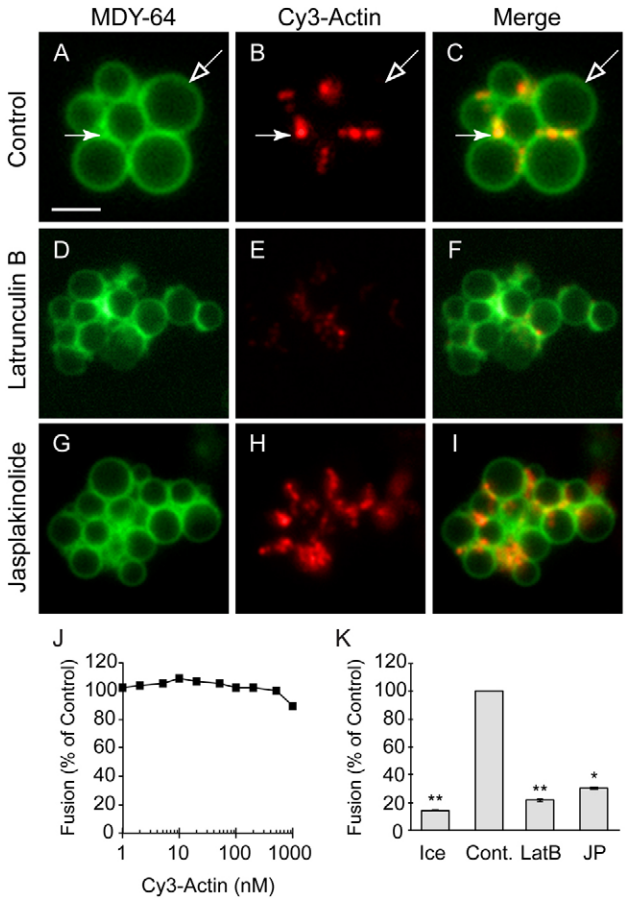

Fig. 1. Actin is enriched at the vertices of docked vacuoles. Vacuoles purified from the yeast strain DKY6281 were incubated under docking conditions for 30 minutes at 27℃ with 15 nM Cy3–actin. Docking reactions were treated with DMSO (carrier) (**A**–**C**), 0.5 mM LatB (**D**–**F**) or 0.5 mM JP (**G**–**I**). After incubation, the reaction tubes were placed on ice and the vacuoles were stained with 0.5 µM MDY-64, mixed with agarose and prepared for fluorescence microscopy observation. Filled arrows are examples of vertex sites. Open arrows are examples of outer edge membranes. Scale bar: 2 µm. (**J**) Fusion reactions containing 3 µg each of vacuoles from BJ3505 (*PHO8 pep4*Δ) and DKY6281 (*pho8*Δ *PEP4*) were treated with purified Cy3-labeled yeast actin at the indicated concentrations and incubated for 90 minutes at 27℃ (n=3). Fusion was tested by content mixing and measuring Pho8p activity. Data represent mean values (±s.e.m.) normalized so that the no treatment reaction equals 100% (n=3). (**K**) Fusion reactions were treated with 0.5 mM JP, 0.5 mM LatB, or DMSO and incubated for 90 minutes at 27℃ (n=3). Data represent mean values normalized to the DMSO-treated reaction (±s.e.m.).

whereas stabilizing F-actin with JP caused a striking increase in vertex labeling with Cy3–actin (Fig. 1G–I). Taken together, these findings showed that vertex enrichment of Cy3–actin could reflect the state of polymerization. Fig. 1J shows a dose–response curve of Cy3–actin on vacuole fusion. We found that Cy3–actin did not alter fusion at any of the tested concentrations. When LatB and JP were tested for their effects on content mixing we found both compounds potently inhibited fusion as described previously (Eitzen et al., 2002) (Fig. 1K).

To quantify the enrichment of Cy3–actin at vertices, we used ratiometric fluorescence microscopy that compares the fluorescence intensity of Cy3–actin to that of MDY-64. The

clustering of vacuoles and formation of docking sites leads to the doubling of membrane staining at the points of contact relative to the outer edge where membranes are not in contact with other vacuoles. Thus, differences in the relative amounts of membranes between the domains of docked vacuoles must be normalized through the use of ratiometric microscopy. First, maximum pixel intensities of Cy3–actin and MDY-64 were measured at each vertex site and expressed as a ratio of Cy3–actin to MDY-64 ($Vertex^{Cy3}$:$Vertex^{MDY\text{-}64}$). The ratio of Cy3–actin to MDY-64 was next measured at the outer edges of the docked vacuoles ($Outer\ edge^{Cy3}$:$Outer\ edge^{MDY\text{-}64}$). The ratios of Cy3 to MDY at vertices were determined by dividing each vertex ratio by the normalized geometric mean of the Cy3 to MDY ratios at the outer edges. Ratios were determined for every vertex in at least ten clusters of docked vacuoles. In Fig. 2A, we show the ratiometric data for untreated control reactions, as well as those treated with JP and LatB. Each vertex ratio was plotted in a cumulative distribution plot depicting the percentile values of the Cy3–actin:MDY-64 ratios for each of the conditions. Each ratio in a dataset was ordered and plotted against the percentile rank of the values. The ratios of Cy3–actin enrichment in untreated control reactions ranged from 1 to a maximum of ~13 (Fig. 2A, black circles). When vacuoles were treated with JP, it caused a marked increase in the number of vertices enriched with Cy3–actin causing a substantial right-shift in the distribution curve with enrichment ratios up to ~25:1 (Fig. 2A, gray circles). By contrast, treatment with LatB caused a reduction in Cy3–actin enrichment and a left-shifted curve (Fig. 2A, empty circles). Fig. 2B shows the geometric means and 95% confidence intervals for the ratios in Fig. 2A. These are lower boundary of estimates of vertex enrichment owing to asynchronous reactions of individual vacuoles within a cluster.

We next determined whether changes in vertex enrichment were accompanied by a parallel change in Cy3–actin incorporation onto the vacuoles. The docking reactions were performed as above using 0.3 μM Cy3–actin. After incubation we performed membrane fractionations and fluorometry in lieu of microscopy. Vacuoles were re-isolated by centrifugation and the unbound Cy3–actin was collected with the supernatant. The vacuole fractions were then resuspended in a volume of buffer equivalent to the starting reaction and solubilized with Thesit. Supernatants were also treated with equal volumes of Thesit. Both vacuole and supernatant fractions were analyzed using a

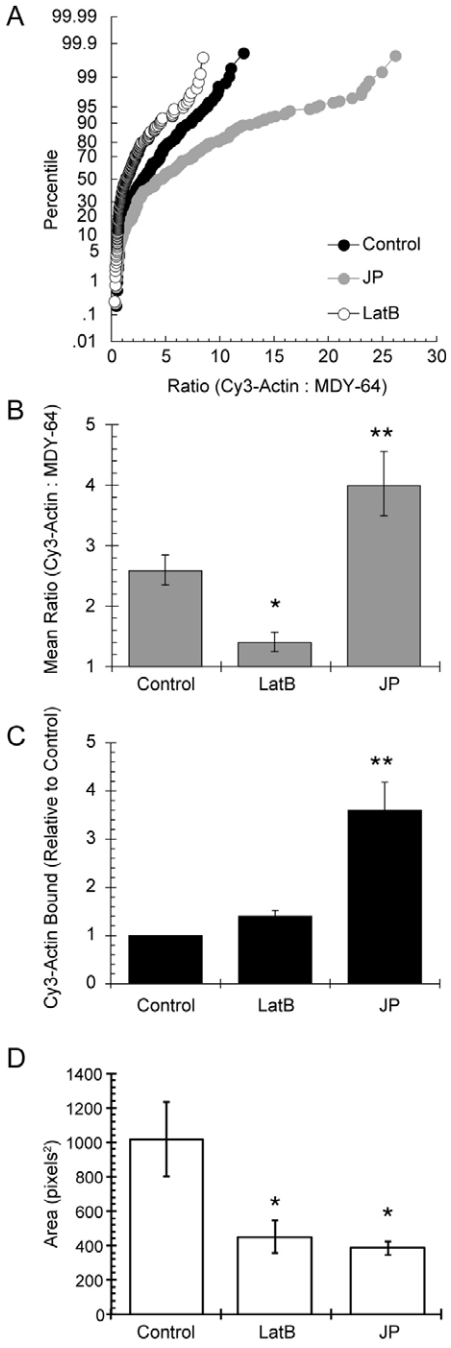

Fig. 2. Quantification of Cy3–actin vertex enrichment and membrane association. Docking reactions were performed as in Fig. 1. (**A**) Cumulative distribution plots show the percentile values of Cy3–actin to MDY-64 ratios for each vertex under the indicated treatments. Each curve is compiled from at least ten vacuole clusters where the maximum pixel intensity was determined for every vertex and midpoint of the outer edge membrane. Pixel intensities were measured in both fluorescence channels at each subdomain and expressed as a ratio of Cy3–actin to MDY-64. Outer edge ratios were normalized to a value of 1 and the enrichment of Cy3–actin at vertices were expressed relative to outer edge intensities. Each ratio in a dataset was ordered and plotted against the percentile rank of the values. (**B**) The data from A is plotted to show the geometric means with their 95% confidence intervals. (**C**) To measure the total incorporation of Cy3–actin onto vacuoles, docking reactions were incubated with 0.3 μM Cy3–actin for 30 minutes at 27℃. After incubation, the reactions were separated into vacuole and supernatant fractions by centrifugation (13,000 ***g***, 5 minutes, 4℃). Supernatants were placed in new tubes and vacuole pellets were resuspended in a volume of PS buffer equal to the starting reaction volume. Both fractions were mixed with 100 μl of 4 mM Thesit detergent. The Cy3–actin fluorescence was measured for each fraction using a BMG Labtech POLARstar Omega plate reader exciting at 546 nm and recording emission at 570 nm. Cy3–actin binding to control reactions (DMSO) was normalized to 1. Cy3–actin binding in the presence of LatB and JP were expressed as values relative to the control. Error bars indicate s.e.m. (n=3). (**D**) To visualize vacuole fusion using fluorescence microscopy, vacuole fusion reactions were treated with either DMSO, 0.5 mM JP, 0.5 mM LatB and incubated for 90 minutes. Reaction samples were stained with MDY-64 and transferred onto microscope slides for fluorescence microscopy examination. The area of vacuole cross sections were measured for each vacuole in a cluster. Ten wide-field images containing 10–15 clusters were measured for each condition using ImageJ. Vacuole area is expressed at $pixels^2$. Data represent the geometric means of vacuole areas with their 95% confidence intervals. *P<0.001, **P<0.00001 for differences relative to control.

fluorescence plate reader, and the amount of incorporated Cy3–actin was calculated as a percentage of the total input. On average, untreated control reactions bound to ~20% of the 0.3 μM Cy3–actin input and were normalized to 1. When normalized to untreated control reactions, we found that LatB had little effect on the amount of Cy3–actin associated with the membrane, whereas vertex enrichment was markedly inhibited. This suggests that LatB did not inhibit actin binding to the vacuole and that G-actin was dispersed on docked vacuoles (Fig. 2C). Unlike the effect of LatB, JP treatment caused a fourfold increase in Cy3–actin binding. Taken together these data indicate that the vacuole actively incorporated Cy3–actin, and that the increased incorporation was proportional to the formation of F-actin filaments. To visualize the inhibition of fusion by LatB and JP, we monitored fusion by measuring vacuole size (Merz and Wickner, 2004b). Fusion reactions were incubated with DMSO (control), LatB or JP for 90 minutes at 27℃. Samples were then stained with FM4-64, transferred onto microscope slides and imaged using fluorescence microscopy. We found that reactions treated with DMSO showed an increase in vacuole size, indicating that fusion had occurred, whereas those treated with LatB and JP remained small showing that fusion was inhibited (Fig. 2D).

SNAREs and HOPS regulate actin enrichment

Previous studies have shown that treating vacuoles with JP inhibited the vertex enrichment of SNAREs and HOPS on docked vacuoles (Wang et al., 2003). In addition, that study found that recapturing free SNAREs into cis-complexes reduced DNase-I (G-actin) accumulation at vertices. However, it was not determined whether F-actin formation was activated or whether actin was simply dispersed. Here, we used Cy3–actin to trace endogenous pools and determined whether the fusion machinery regulated the vertex accumulation of Cy3–actin, as well as its incorporation onto vacuolar membranes. Although anti-Vam7p antibody had no effect on actin accumulation at the vertex, we found that using anti-Vam3p antibody or an excess of Sec17p, caused a striking reduction in Cy3–actin vertex accumulation of 50% and 75%, respectively (Fig. 3G, $P<0.01$ and 0.00001, respectively). An excess of Sec17p recaptures primed SNAREs into cis-SNARE bundles (Wang et al., 2000), suggesting that the actin enrichment occurred downstream of SNARE priming. Because anti-Vam3p antibody inhibits SNARE complex formation (Fratti and Wickner, 2007; Fratti et al., 2007), we can deduce that the actin enrichment at vertices occurred after SNAREs initiated docking. The effect of Sec17p was consistent with a previous report that used 4 μM Rhodamine-labeled rabbit actin to monitor actin dynamics on yeast vacuoles (Eitzen et al., 2002). However, the effect of Sec17p in our experiments was not as pronounced as that shown in the previous report. This is possibly because of a weaker binding affinity between rabbit actin and yeast actin, which was reflected in the need for greater than two orders of magnitude more rabbit actin to label the vertex ring relative to the 15 nM Cy3–actin required for labeling.

When tethering was blocked with antibodies that target the HOPS subunit Vps33p or the Rab GTPase Ypt7p, we observed an intermediate level of inhibition ($P<0.05$). Taken together, these data illustrate that actin enrichment occurred after priming and continued through the docking stage. Differences in vertex enrichment were not due to changes in the incorporation of Cy3–actin. As seen in Fig. 3H, Cy3–actin incorporation was unchanged regardless of the treatment used. This illustrates that the fusion machinery regulated the vertex enrichment of actin, but not its polymerization equilibrium. Fig. 3I shows the inhibition of fusion by each of the treatments used above. Each of

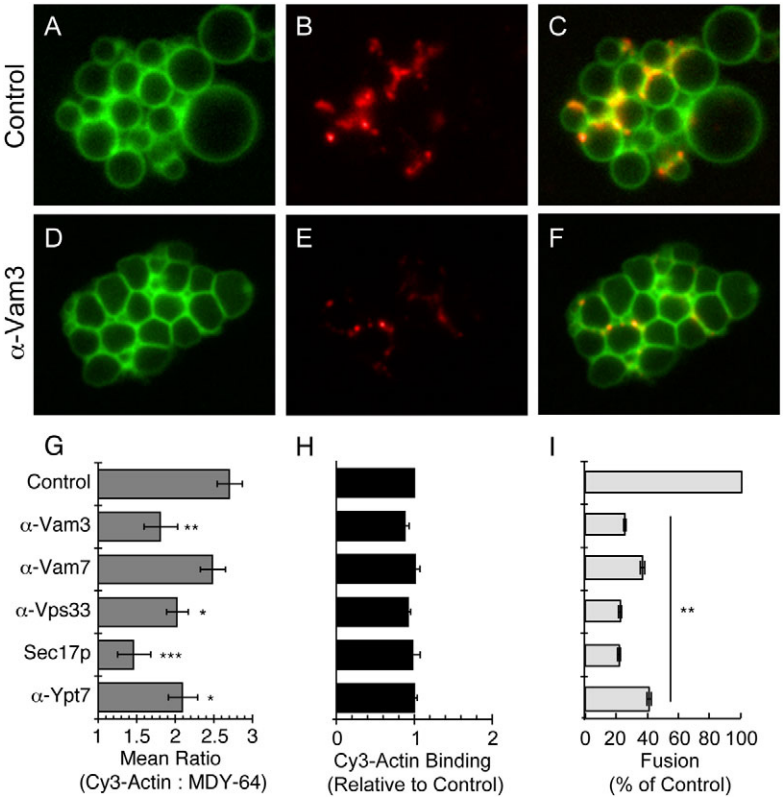

Fig. 3. SNAREs, HOPS and Ypt7 regulate Cy3–actin enrichment at the vertices of docked vacuoles. Vacuoles were incubated under docking conditions as described in Fig. 1 and treated with either buffer (**A**–**C**), or 190 nM anti-Vam3p antibody (**D**–**F**). After incubation, reaction tubes were placed on ice and the vacuoles were stained with MDY-64, mixed with agarose and transferred onto glass slides for observation by fluorescence microscopy. (**G**) Docking reactions were incubated with 15 nM Cy3–actin and treated with buffer or 190 nM anti-Vam3p antibody, 150 nM affinity-purified anti-Vam7p antibody, 32 nM affinity purified anti-Vps33p antibody, 750 nM Sec17p or 133 nM affinity purified anti-Ypt7p antibody. Reactions were incubated for 30 minutes at 27℃, then placed on ice, labeled with MDY-64 and prepared for microscopy. Shown are the geometric mean values±95% confidence intervals of the relative enrichments. (**H**) Parallel reactions to those described for G were incubated with 0.3 μM Cy3–actin. After incubation, the reactions were separated into membrane and supernatant fractions as described in Fig. 2. Fluorescence of both fractions was measured. Cy3–actin binding to control reactions was normalized to 1. Cy3–actin binding in the presence of inhibitors was expressed as values relative to the control (±s.e.m.; $n=3$). (**I**) Fusion reactions were treated with the inhibitors listed in A and incubated for 90 minutes at 27℃. The data shown represent the mean (±s.e.m.; $n=3$) percentage of vacuole fusion relative to that in the untreated control, which was normalized to 100%. Fusion was measured by determining the level of Pho8p activity. *$P<0.05$, **$P<0.01$, ***$P<0.00001$ for differences relative to control.

the treatments caused a significant ($P<0.01$) block in vacuole fusion as measured by determining Pho8p activity.

Because the fusion machinery controlled the vertex enrichment of actin, we next tested whether the effect of JP on actin localization could be prevented with inhibitors of the pathway or LatB. Vacuole docking reactions underwent two treatments. First, vacuoles were incubated with anti-Vam3p or anti-Ypt7p antibodies, LatB or carrier (DMSO). After incubating for 5 minutes, JP was added to each reaction except the carrier-treated control. Reactions were incubated for a total of 30 minutes and observed by microscopy. As seen in Fig. 3, JP caused a marked increase in Cy3–actin vertex enrichment (Fig. 4A,B, $P<0.0001$). The effect of JP was not blocked by anti-Vam3p antibody ($P>0.05$ relative to JP alone), suggesting that its effects were not linked to SNARE function. Anti-Ypt7p antibody modestly lowered Cy3–actin enrichment relative to JP alone. Although the effect of JP in the presence of anti-Ypt7p antibody was still significantly increased relative to the untreated control ($P<0.0001$), it was reduced relative to JP alone ($P<0.05$). LatB did not alter the effect of JP on actin enrichment ($P>0.05$). These data suggest that although antibodies significantly reduced the mobilization of Cy3–actin to the vertex, the population of actin that reached the vertex was able to continue to polymerize in the presence of JP.

Actin dynamics are regulated by ergosterol and PtdIns(4,5)P_2

Many studies have shown that actin polymerization can be regulated by cholesterol and the phosphoinositide PtdIns(4,5)P_2 (Hao and Bogan, 2009; Kwik et al., 2003; Rozelle et al., 2000). However, most of the evidence has been collected at the plasma membrane, and it is unclear whether lipids control actin dynamics on lysosomal organelles. Until recently it was thought that the human class III phosphoinositide 3-kinase (PI3K) subunit Vps34 (also known as PIK3C3) did not play a role in the regulation of actin remodeling; however, Grinstein and colleagues have reported that both class I and class III PI3Ks play a crucial role in regulating actin polymerization on phagosomal membranes (Bohdanowicz et al., 2010). Here, we determined the effect of regulatory lipids on actin dynamics at the vertex ring. We used lipid-binding ligands and lipid-modifying enzymes to alter the lipid composition of the vertex domain. To bind PtdIns(3)P, we used the FYVE domain from human HRS (also known as HGS). We also used the phosphoinositide 3-phosphatase myotubularin (MTM1) that converts PtdIns(3,5)P_2 and PtdIns(3)P into PtdIns(5)P and PtdIns, respectively. Although both reagents were known to potently inhibit fusion and the vertex enrichment of SNAREs, HOPS and Ypt7p (Fratti et al., 2004), only the FYVE domain had an inhibitory effect on actin enrichment at vertices (Fig. 5A, $P<0.05$). This indicates that PtdIns(3)P, although crucial for fusion, did not play an essential role in actin dynamics on vacuoles. It is probable that the majority of PtdIns(3)P was used for binding the soluble SNARE Vam7p (Boeddinghaus et al., 2002). Binding diacylglycerol with the C1b domain from protein kinase C (PKC) did not have an effect on actin enrichment (Fig. 5A), illustrating that it was not required for actin regulation. Although diacylglycerol is essential for fusion, it is probable that it regulates an independent aspect of fusion that does not overlap with the control of actin.

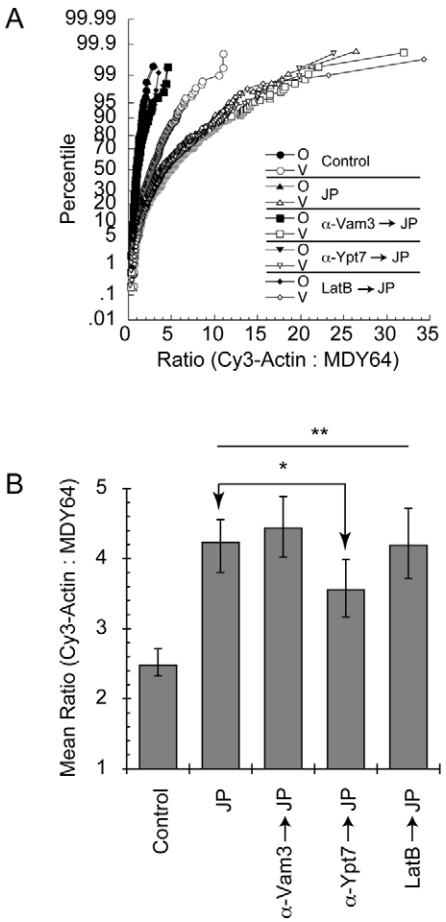

Fig. 4. JP-stimulated actin polymerization is resistant to inhibitors of the fusion pathway. (**A**) Docking reactions were labeled with Cy3–actin and treated with carrier, anti-Vam3 or anti-Ypt7 antibody, or LatB. After incubating for 5 minutes at 27℃ the indicated reactions were additionally treated with JP and incubated for a total of 30 minutes 27℃. After incubation, the vacuoles were stained with MDY-64 and the samples were transferred onto microscope slides for observation by fluorescence microscopy. Shown are the cumulative distribution plots with the percentile values of Cy3–actin to MDY-64 ratios for each vertex (V, open symbols) and outer edge (O, filled symbols) under the indicated treatments. (**B**) Shown are the geometric mean values ± 95% confidence intervals of the relative enrichments. *$P<0.05$ for differences between JP treatment and treatment with anti-Ypt7 antibody followed by JP. **$P<0.0001$ for differences relative to the untreated control.

We next tested the role of ergosterol on actin dynamics. When docking reactions were treated with filipin to bind ergosterol we found that vertex sites were severely depleted of actin, with a 75% reduction relative to the untreated control (Fig. 5A, $P<0.00001$). This demonstrated that ergosterol was crucial for the vertex enrichment of actin. Interestingly, filipin did not affect the amount of Cy3–actin binding (Fig. 5B), suggesting that ergosterol was required for the mobilization and accumulation of actin in microdomains but not the level of actin incorporation. Fig. 5C shows the inhibition of fusion by each of the treatments used above. Each of the treatments caused a significant block in vacuole fusion.

The lipid PtdIns(4,5)P_2 has been shown to regulate actin polymerization through the activation of Wiskott–Aldrich syndrome protein (WASP) family members (Rohatgi et al.,

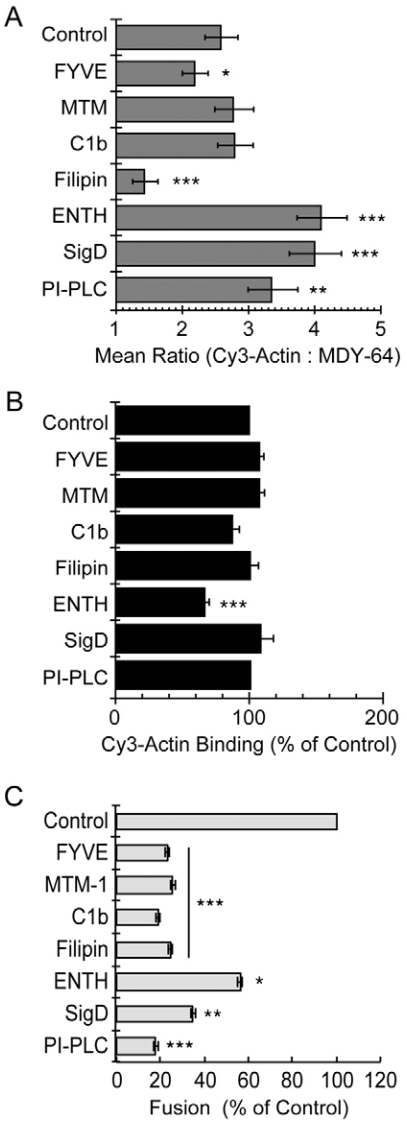

Fig. 5. Ergosterol and PtdIns(4,5)P_2 regulate Cy3–actin enrichment at the vertices of docked vacuoles. (**A**) Docking reactions were labeled with 15 nM Cy3–actin and treated with buffer or 1 μM FYVE, 1 μM MTM1, 10 μM C1b, 20 μM filipin, 30 μM ENTH, 2 μM SigD or 1 U/ml PI-PLC. Reactions were incubated for 30 minutes at 27℃, then placed on ice and labeled with MDY-64, and prepared for microscopy. Shown are the geometric mean values ± 95% confidence intervals of the relative enrichments. (**B**) Parallel reactions to those described in A were incubated with 0.3 μM Cy3–actin. After incubation, the reactions were separated into membrane and supernatant fractions as described in Fig. 2. Fluorescence of both fractions was measured. Cy3–actin binding to control reactions was normalized to 100%. Cy3–actin binding in the presence of inhibitors was expressed as values relative to the control. Error bars indicate s.e.m. (n=3). (**C**) Fusion reactions were treated with the inhibitors listed in A and B. Reactions were incubated for 90 minutes at 27℃ and fusion was measured by determining the level of Pho8 activity. Error bars indicate s.e.m. (n=3). *P<0.05, **P<0.001, ***P<0.00001 for differences relative to control.

2000). In yeast, the WASP homolog Las17p is known to regulate fusion (Eitzen et al., 2002). This suggests that PtdIns(4,5)P_2 can play an important role in regulating vacuolar actin dynamics. This notion is further supported by a study that showed that the phosphatidylinositol-specific phospholipase C (PLC) inhibitor U73122 stimulates actin polymerization (Isgandarova et al., 2007), presumably through an increase in PtdIns(4,5)P_2. Interestingly, U73122 also inhibits vacuole fusion (Jun et al., 2004), suggesting that the levels of PtdIns(4,5)P_2 and F-actin have to be carefully regulated to promote fusion. Here, we tested the role PtdIns(4,5)P_2 in regulating actin dynamics during vacuole fusion. For this we treated docking reactions with the ENTH domain from the PtdIns(4,5)P_2 ligand epsin-1 (hereafter designated ENTH), or the PtdIns(4,5)P_2 5-phosphatase SigD. Both have been shown to inhibit fusion and inhibit the vertex enrichment of SNAREs, Ypt7p, HOPS, PtdIns(3)P and ergosterol (Fratti et al., 2004). Unexpectedly, ENTH and SigD augmented actin vertex enrichment relative to the untreated control (Fig. 5A, P<0.00001 for each). Many studies have found that PtdIns(4,5)P_2 is essential for actin polymerization, and that reducing the availability of PtdIns(4,5)P_2 through ligation, enzymatic treatments or cluster dispersal through the extraction of cholesterol all inhibit actin polymerization (Rozelle et al., 2000; Szymanska et al., 2008; van Rheenen et al., 2007). However, we must remain aware that vertex enrichment does not linearly correlate with polymerization. It is possible that reducing free PtdIns(4,5)P_2 enhances the vertex enrichment of actin, independent of its effects on polymerization. When we examined the amount of total Cy3–actin incorporation, we found that ENTH reduced actin binding (Fig. 5B). The opposing effects of ENTH on Cy3–actin vertex enrichment and binding suggests that the role of PtdIns(4,5)P_2 on actin binding and enrichment are separable. Moreover, this indicates that the effect on ENTH on Cy3–actin vertex enrichment is an underestimation of the differences between the control and the ENTH-treated reaction. We also tested the PtdIns-specific PLC (PI-PLC), which potently inhibits fusion and the vertex enrichment of Ypt7p and PtdIns(3)P (Fratti et al., 2004; Mayer et al., 2000) (Fig. 5C). Treating vacuoles with PI-PLC also caused an increase in Cy3–actin enrichment at the vertex (Fig. 5A, P<0.001) without altering the amount of Cy3–actin bound to the membrane. These treatments all limit the amount of free PtdIns(4,5)P_2 and cause the enhancement of Cy3–actin enrichment without altering the level of actin incorporation at the end of the reaction. Taken together, these studies suggest that actin polymerization on lysosomes can be regulated by an alternate mechanism relative to the plasma membrane.

Actin polymerization and PtdIns(4,5)P_2 enrichment

The influence of PtdIns(4,5)P_2 on actin polymerization has been well described in many systems. However, our data indicates that this lipid had a negative effect on actin enrichment at the vertex ring. To further investigate the relationship between actin and PtdIns(4,5)P_2 during vacuole fusion, we monitored the distribution and vertex enrichment of this lipid when actin dynamics were altered with LatB and JP. To monitor the dynamics of PtdIns(4,5)P_2, we recombinantly expressed the ENTH domain from epsin-1 and conjugated it to Cy3 for ratiometric fluorescence microscopy experiments. Previously, we found that PtdIns(4,5)P_2 became enriched at the vertices of docked vacuoles; however, we did not examine the regulation of its enrichment (Fratti et al., 2004). Others have also found vacuole pools of PtdIns(4,5)P_2 in vivo (Wiradjaja et al., 2007). Here, we show that PtdIns(4,5)P_2 became enriched at the vertices of docked vacuoles (Fig. 6A–C), and that enrichment was augmented when vacuoles were treated with JP (Fig. 6D–F). This suggested that F-actin stabilization applied positive regulation on PtdIns(4,5)P_2 enrichment into

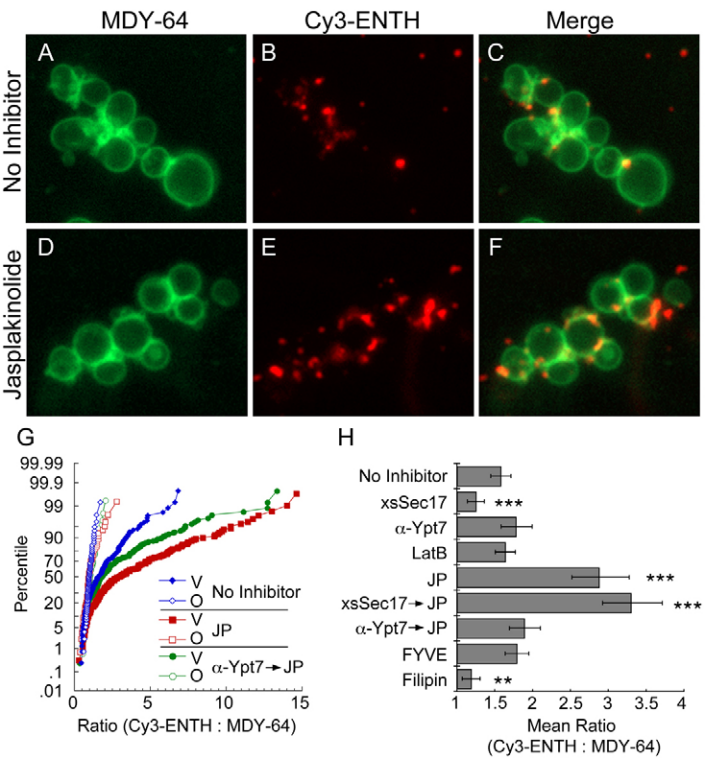

Fig. 6. F-actin-regulated PtdIns(4,5)P_2 enrichment at vertex sites. Vacuoles were incubated under docking conditions for 30 minutes at 27℃ with 0.6 μM Cy3–ENTH. Docking reactions were treated with either DMSO (carrier) (**A**–**C**) or 0.5 mM JP (**D**–**F**). After incubation, vacuoles were stained with MDY-64, mixed with agarose and prepared for fluorescence microscopy. (**G**) Cumulative distribution plots show the percentile values of the Cy3–ENTH to MDY-64 ratios for each vertex (V, filled symbols) and outer edge (O, open symbols) for reactions treated with buffer (blue diamonds), JP (red squares) or anti-Ypt7p antibody before JP (green circles). (**H**) Docking reactions were labeled with 0.6 μM Cy3–ENTH and treated with buffer or 750 nM Sec17p, 133 nM affinity-purified anti-Ypt7p antibody, 0.5 mM LatB, 0.5 mM JP, 1 μM FYVE or 20 μM filipin. Separate reactions received Sec17p or anti-Ypt7p before JP treatment. Reactions were incubated for 30 minutes at 27℃, then placed on ice and labeled with MDY-64, and prepared for microscopy. Shown are the geometric mean values ± 95% confidence intervals of the relative enrichments. *P<0.001, **P<0.0001 for differences relative to control.

microdomains. It is possible that PtdIns(4,5)P_2 accumulated at the early vertex and that JP prevented diffusion from the domain. LatB had no effect on PtdIns(4,5)P_2 enrichment at the vertex (Fig. 6H). In addition, PtdIns(4,5)P_2 localization was not inhibited by anti-Ypt7p antibody or the FYVE domain. This suggests that PtdIns(4,5)P_2 enriches at vertices before Ypt7p-dependent tethering occurs. Treatment with excess Sec17p strongly inhibited PtdIns(4,5)P_2 enrichment indicating that SNARE function was required (Fig. 6H). Taken together, these data indicate that PtdIns(4,5)P_2 enrichment occurs between tethering and trans-SNARE pairing, and that actin might polymerize before accumulating at the vertex.

Binding ergosterol also inhibited PtdIns(4,5)P_2 enrichment, which was consistent with its effects on Cy3–actin enrichment as well as reports showing that sterol-rich microdomains are essential for PtdIns(4,5)P_2 clustering (Kwik et al., 2003). Because JP augmented PtdIns(4,5)P_2 enrichment, we examined whether the effect was dependent on the fusion machinery. We found that blocking Rab-dependent tethering with anti-Ypt7p blocked the effect of JP on PtdIns(4,5)P_2 enrichment (Fig. 6H). This is consistent with the results in Fig. 4, showing that anti-Ypt7p antibody reduced the effect of JP on actin enrichment. This further suggests that although vacuoles treated with JP bypass the block caused by excess Sec17p, they remain sensitive to anti-Ypt7p antibody.

Actin colocalization with PtdIns(4,5)P_2

In a previous study it was shown that Cy3–actin colocalized with the HOPS subunit Vps33p, as well as the regulatory lipid PtdIns(3)P (Jun et al., 2006). Because the regulatory lipid PtdIns(4,5)P_2 and actin exhibited an interdependent regulation of their vertex enrichment, we examined whether the two factors colocalized simultaneously at the vertices of docked vacuoles. We performed triple labeling experiments with MDY-64 to stain the entirety of the vacuole clusters, Cy3–actin and a Cy5-labeled ENTH domain. We found that Cy3–actin and Cy5–ENTH colocalized at vertex sites indicating that the lipid PtdIns(4,5)P_2 was present at the same time as actin on docked vacuoles (Fig. 7).

Discussion

The role of actin dynamics in membrane trafficking and fusion is not well defined. Here, we have shown that the core fusion machinery regulates the assembly of actin-rich domains and that its vertex enrichment is separable from actin binding and polymerization. Specifically, we found that actin domains accumulate at the vertices of docked vacuoles, and that actin enrichment is inhibited in the presence of agents that block the activity of SNAREs, Ypt7p and HOPS. Furthermore, we found that the regulatory lipids ergosterol, PtdIns(4,5)P_2 and PtdIns(3)P influence the enrichment of actin on the vertices of docked vacuoles. Although the mechanisms of actin regulation during the fusion pathway remain unclear, we posit that vacuoles need to reach the docking stage, when SNAREs form trans-complexes to stimulate the enrichment of actin. The ability of SNAREs to accomplish this is tied to the function of Ypt7p and HOPS, as well as ergosterol and phosphoinositides. The data presented here also indicates that the location of actin-rich domains is important for fusion and that the formation of F-actin has to be focused in the area where the fusion machinery is located.

Actin and regulatory lipids

In many membrane trafficking pathways actin undergoes polymerization in a manner dependent on cholesterol and phosphoinositides including PtdIns(4,5)P_2 and 3-phosphoinositides

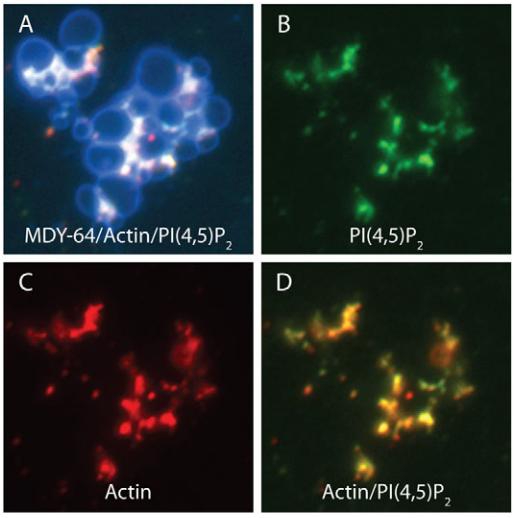

Fig. 7. Actin colocalized with PtdIns(4,5)P_2 at the vertices of docked vacuoles. Docking reactions were incubated with 15 nM Cy3–actin and 0.3 μM Cy5–ENTH for 30 minutes at 27°C. At the end of the incubation, the reactions tubes were transferred onto ice and the vacuoles were stained with MDY-64. Samples were transferred onto microscope slides for observation by fluorescence microscopy. MDY-64, Cy3–actin Cy5–ENTH images were pseudocolored blue, red and green, respectively.

(Bohdanowicz et al., 2010; Rozelle et al., 2000). In our study, the enrichment of actin at vertex sites was regulated by ergosterol, PtdIns(3)*P* and PtdIns(4,5)P_2, yet the incorporation of actin only appeared to be linked to PtdIns(4,5)P_2. It is also worth noting that the experiments performed here were endpoint assays and did not follow the kinetics of polymerization. Thus, it is possible that these lipids also regulate the rate of polymerization without affecting the eventual formation of actin-enriched domains. To our knowledge, the role of these lipids has not been directly examined in the context of regulating the kinetics of actin accumulation at microdomains. Recently, Eitzen and colleagues showed that bulk actin polymerization occurs rapidly during in vitro vacuole fusion (Isgandarova et al., 2007). They also found that polymerization was enhanced when Plc1p (the yeast phospholipase C) activity was inhibited with U73122, suggesting that increased levels of PtdIns(4,5)P_2 stimulated actin polymerization. However, the effect of U73122 on the rate of actin polymerization was not measured. U73122 is an inhibitor of fusion that functions during priming (i.e. early in the reaction pathway) (Jun et al., 2004), suggesting that actin polymerization could occur prematurely and inhibit fusion. In essence, this would mimic the effect of JP. Taken together with our data here and with earlier studies showing that U31722 inhibits vacuole fusion, it is possible that the enhanced polymerization occurs in domains outside of the vertex ring. This would be consistent with the notion that actin polymerization must be localized to the vertex after docking.

The link between actin dynamics and PtdIns(3)*P* is a newly discovered aspect of cytoskeletal organization. Grinstein and colleagues have reported that 3-phosphoinositides regulate actin polymerization on phagosomal membranes by feeding into the synthesis of PtdIns(3,4)P_2 and PtdIns(3,4,5)P_3 (Bohdanowicz et al., 2010). In our studies, we found that free PtdIns(3)*P* was required for native actin dynamics at the vertex ring of vacuoles. Interestingly, we had previously observed a link between PtdIns(3)*P* and actin. When probing for PtdIns(3)*P* with Cy3–FYVE, LatB was previously found to cause a striking increase in the amount of vertex localized PtdIns(3)*P* (Fratti et al., 2004). This was in contrast to the effects of JP, which inhibited the PtdIns(3)*P* localization to the vertex ring. Taken together, these data indicate that there is a substantial connection between actin dynamics and 3-phosphoinositides, and that the localization of PtdIns(3)*P* is inversely proportional to the enrichment of F-actin at vertex sites.

Actin and PtdIns(4,5)P_2 localization

In this study we found that PtdIns(4,5)P_2 negatively regulates the vertex enrichment of actin. We also found that treating vacuoles with JP augmented the vertex enrichment of PtdIns(4,5)P_2, suggesting that actin filaments enhance the vertex enrichment of PtdIns(4,5)P_2. JP has been reported to enhance co-clustering of raft-associated proteins on T cells (Chichili and Rodgers, 2007; Chichili et al., 2010), suggesting that JP could be mediating clustering of PtdIns(4,5)P_2 microdomains on docked vacuoles. Furthermore, both T-cell domains and vacuolar PtdIns(4,5)P_2 domains are sensitive to filipin treatment. Previous studies using JP and vacuoles have shown that Q-SNAREs, HOPS and PtdIns(3)*P* are blocked from the vertex, whereas Ypt7p localization is not affected (Fratti et al., 2004; Wang et al., 2003), indicating that actin only controls a subset of the fusion machinery. These data along with previous reports are consistent with the actin fence model where particular proteins are contained within a perimeter of F-actin filaments (Tamkun et al., 2007). We posit that the stabilization of F-actin by JP at early timepoints in the fusion process prevents the trapping of SNAREs within actin fences.

Actin, membrane deformation and fusion

There are several hypotheses on the role of actin during fusion. One model proposes that the function of actin lies in the deformation of the membrane. A second model suggests that actin depolymerization occurs to permit the docking of vesicles before fusion, whereas re-polymerization aids in concentrating, or corralling, membrane proteins into microdomains. These models are not mutually exclusive and might be different aspects of a multifaceted mechanism. Recently, Liebl and Griffiths showed that actin polymerization could either activate or inhibit the fusion of phagosomes with lysosomes (Liebl and Griffiths, 2009). They showed that actin patches blocked the docking of phagosomes with lysosomes and that docking and fusion were restored after actin had depolymerized. Interestingly, when phagosomes contained budding yeast, they found that actin accumulated at the negatively curved portion of the phagosomal membrane around the neck of the yeast bud. This is similar to findings showing that in *Dictyostelium discoideum* actin filaments push into the negatively curved domains of phagosomes containing budded yeast where the force generated by actin causes the scission of the vesicle and its cargo (Clarke et al., 2010). Thus, it is probable that negative membrane curvature promotes actin polymerization or stabilizes actin filaments. In vacuole homotypic fusion, vacuoles are thought to undergo a hemifusion state where the outer leaflets of the docked vacuoles fuse into a continuous membrane while the inner leaflets remain separate (Reese and Mayer, 2005; Reese et al., 2005). When vacuoles initially dock, the membranes bend to create high positive curvature at the vertex ring. The two membranes with positive curvature become negatively curved upon hemifusion. Thus, it is possible that the accumulation of actin at vertices occurs after hemifusion. Liebl and Griffiths also showed that actin

polymerization induces negative curvature on macropinosomes. Therefore, it is also possible that actin could participate in the progression between docking and hemifusion by inducing negative curvature at the vertex ring (Liebl and Griffiths, 2009).

Other investigators have examined the distortion of membranes using vesicles coated with ActA, a protein from the bacterium *Listeria monocytogenes* that activates actin polymerization and generates actin comet tails on membranes (Giardini et al., 2003; Upadhyaya et al., 2003). Both groups have shown that actin filaments can push and hold the vesicle membranes, which causes vesicle deformation. Actin filaments push into the membrane in a direction that is orthogonal to the comet formation and vesicle movement while filaments at the lagging tip deform the membrane in the opposite direction of motion resulting in a teardrop shape. The coupled effects of the deformation lead to the formation of a vesicle tip with a pronounced positive curvature. If we apply this model to the role of actin in vacuole fusion, we posit that actin filaments could push and pull at the vertex domain and deform the membrane to create increased positive curvature similar to the lagging tip of a comet-driven endosome, as well as creating negative curvature on both sides of a vertex extension coupled with the force generated by trans-SNARE complexes. This could drive the transition between docking and hemifusion. Although these deformations are too small to be visualized by light microscopy, their occurrence might be inferred by examining other properties. For instance, the lipid composition of the vertex ring requires both negative and positive curvature. Diacylglycerol, phosphatidic acid and ergosterol induce negative curvatures in membranes, whereas PtdIns(4,5)P_2 and other phosphoinositides induce positive curvatures in membranes. Although these lipids coexist in the vertex ring, it is likely that two environments with opposite curvatures exist adjacently as part of a larger complex of subdomains. Thus, it is possible that actin facilitates the formation of a compound vertex microdomain where both positive and negative curvatures can exist before hemifusion.

Materials and Methods

Reagents

Reagents were dissolved in PS buffer (20 mM PIPES-KOH pH 6.8, 200 mM sorbitol) with 125 mM KCl unless indicated otherwise. Anti-Vam3p (Nichols et al., 1997), anti-Vam7p (Ungermann and Wickner, 1998), anti-Ypt7p (Mayer and Wickner, 1997) and anti-Vps33p (Seals et al., 2000) antibodies, His_6–Sec17p (Haas and Wickner, 1996), FYVE (Gillooly et al., 2000), His_6–MTM1 (Taylor et al., 2000), C1b (Johnson et al., 2000), ENTH (Rosenthal et al., 1999) and His_6–SigD (Marcus et al., 2001) were described previously. FYVE, C1b and ENTH were first produced as GST fusions, after which the GST tags were removed by protease cleavage using factor-Xa (New England Biolabs) or thrombin (Amersham Biosciences) according to the manufacturers' protocols. Factor Xa and thrombin were removed with *p*-aminobenzamidine-agarose (Sigma) in PS buffer. PI-PLC (from *Bacillus cereus*; Sigma) was dissolved in PS buffer with 125 mM KCl and 5 mM $MgCl_2$. Filipin III, LatB and JP were purchased from Sigma and BIOMOL and dissolved in DMSO. ENTH was labeled with either Cy3 or Cy5 NHS ester (GE Healthcare) according to the manufacturer's protocol and dialyzed in to PS buffer with 125 mM KCl.

Actin preparations

Yeast actin was prepared as described (Goode, 2002; Jun et al., 2006). DKY6281 was grown in six liters of YPD at 30℃ until OD_{600}=6–8. Cells were washed twice in G-buffer (10 mM Tris-HCl pH 8, 0.2 mM $CaCl_2$, 2 mM DTT and 0.5 mM ATP) and frozen dropwise in liquid nitrogen. Frozen cell pellets in liquid nitrogen were lysed using a Waring blender. Lysates were thawed in G-buffer in the presence of protease inhibitors and clarified by centrifugation. Low speed centrifugation in a JA-20 rotor (13,400 ***g***, 4℃, 30 minutes) was followed by ultracentrifugation (60Ti rotor, 45,000 r.p.m., 120 minutes, 4℃) after which the supernatants were filtered through cheesecloth and loaded on to a 40 ml column of affigel-10 linked DNase-I. Cytosol was passed through the DNase-I column at 2 ml per minute. The column was washed with 50 ml G-buffer with protease inhibitors and 10% deionized formamide. Two more washes were performed using 50 ml G-buffer with protease inhibitors, 10% deionized formamide and 0.2 M NH_4Cl followed by 50 ml G-buffer alone. Actin was eluted with 50 ml G-buffer with protease inhibitors and 50% deionized formamide, and dialyzed in PS buffer with 125 mM KCl and 5 mM $MgCl_2$. Actin was covalently labeled with Cy3 NHS ester (GE Healthcare) according to the manufacturer's protocol.

Vacuole isolation and in vitro vacuole docking

Vacuoles were isolated from the *S. cerevisiae* strain DKY6281 as described previously (Haas et al., 1994). Standard in vitro docking reactions (30 µl) contained 6 µg of vacuoles, docking buffer (20 mM PIPES-KOH pH 6.8, 200 mM sorbitol, 100 mM KCl, 0.5 mM $MgCl_2$), an ATP-regenerating system (0.3 mM ATP, 0.7 mg/ml creatine kinase, 6 mM creatine phosphate), 20 µM coenzyme A (CoA), and 283 nM inhibitor of protease B (IB_2) and either 15 nM Cy3–actin, 0.6 µM Cy3–ENTH or 0.3 µM Cy5–ENTH. Reactions were incubated at 27℃ for 30 minutes and placed on ice and stained with 0.5 µM MDY-64 (Invitrogen). Reactions were next mixed with 50 µl of 0.6% low-melt agarose (in PS buffer), vortexed to disrupt spurious clustering and mounted on slides for observation by fluorescence microscopy.

In vitro vacuole fusion

In vitro content-mixing fusion reactions (30 µl) contained 3 µg each of vacuoles from BJ3505 (*PHO8 pep4*Δ) and DKY6281 (*pho8*Δ *PEP4*) backgrounds, fusion reaction buffer (20 mM PIPES-KOH pH 6.8, 200 mM sorbitol, 125 mM KCl, 5 mM $MgCl_2$), an ATP-regenerating system (1 mM ATP, 0.1 mg/ml creatine kinase, 29 mM creatine phosphate), 10 µM CoA, and 283 nM IB_2. Fusion was determined by the activation of pro-alkaline phosphatase (proPho8p) by the protease Pep4p. Fusion reaction mixtures were incubated at 27℃ for 90 minutes, after which the vacuoles were lysed in 250 mM Tris-HCl pH 8.5, 0.4% Triton X-100, 10 mM $MgCl_2$, and 1 mM *p*-nitrophenyl phosphate. Mature Pho8p activity was assayed through the dephosphorylation of *p*-nitrophenyl phosphate and generation of *p*-nitrophenolate. Fusion units were measured by determining the *p*-nitrophenolate produced $min^{-1}\cdot\mu g^{-1}$ per *pep4* vacuole. *p*-Nitrophenolate absorbance was measured at 400 nm.

Microscopy

Images were acquired as described previously (Fratti et al., 2004; Wang et al., 2002; Wang et al., 2003). We used a Zeiss Axio Observer Z1 inverted microscope equipped with a X-Cite 120XL light source, Plan Apochromat 63× oil objective (NA 1.4), and an AxioCam CCD camera. Cy3 images were acquired using a 43 HE CY3 shift-free filter set and MDY-64 images were acquired using a 38 HE EGFP shift-free filter set. Cy5 images were acquired using a 50 HE CY5 shift-free filter set. Image acquisition scripts were used that included fixed exposure times for each label. Images were processed and analyzed using ImageJ software. For ratiometric measurements the maximum pixel values for vertex and outer edge membrane were measured for specific (Cy3–actin or Cy3– or Cy5–ENTH) and non-specific probes in each fluorescence channel. All vertices and outer edge membranes were measured within a vacuole cluster. In each experiment, 15–20 clusters containing a total of 100–300 vertices were analyzed for each treatment in multiple experiments. The data are presented in each figure is a representative experiment. First, pixel ratios of vertex to the outer edge membrane were taken for each fluorescent channel. Pixel ratios for nonspecific labeling were normalized to 1. Next, ratios of specific to nonspecific labels were taken at each vertex and the outer edge membranes, and enrichment was expressed relative to outer edge membrane intensities.

Statistical analysis of actin and ENTH enrichment at vertices was performed using JMP 5 (SAS Institute). Ratio data were log-transformed before analysis to yield near-normal distributions with comparable variances. Ratio means and 95% confidence intervals were analyzed using one-way ANOVAs. Significant differences were determined using Student's *t* test and corrected for multiple comparisons using the Dunn–Sidak method (Sokal and Rohlf, 1994). *P*-values less than 0.05 were considered significant.

Acknowledgements

We thank William Wickner and Gary Eitzen for generous gifts of antisera. We also thank Joanna Shisler for critical reading of the manuscript and helpful discussions.

Funding

This research was supported in part by a Basil O'Connor Starter Scholar Research Award from the March of Dimes Birth Defects Foundation to R.A.F. [research grant number #5-FY09-117] and

startup funds provided to R.A.F. by the University of Illinois at Urbana-Champaign.

References

Albiges-Rizo, C., Destaing, O., Fourcade, B., Planus, E. and Block, M. R. (2009). Actin machinery and mechanosensitivity in invadopodia, podosomes and focal adhesions. *J. Cell Sci.* **122**, 3037-3049.

Babst, M., Odorizzi, G., Estepa, E. J. and Emr, S. D. (2000). Mammalian tumor susceptibility gene 101 (TSG101) and the yeast homologue, Vps23p, both function in late endosomal trafficking. *Traffic* **1**, 248-258.

Boeddinghaus, C., Merz, A. J., Laage, R. and Ungermann, C. (2002). A cycle of Vam7p release from and PtdIns 3-P-dependent rebinding to the yeast vacuole is required for homotypic vacuole fusion. *J. Cell Biol.* **157**, 79-89.

Bohdanowicz, M., Cosio, G., Backer, J. M. and Grinstein, S. (2010). Class I and class III phosphoinositide 3-kinases are required for actin polymerization that propels phagosomes. *J. Cell Biol.* **191**, 999-1012.

Bubb, M. R., Spector, I., Beyer, B. B. and Fosen, K. M. (2000). Effects of jasplakinolide on the kinetics of actin polymerization. An explanation for certain in vivo observations. *J. Biol. Chem.* **275**, 5163-5170.

Chichili, G. R. and Rodgers, W. (2007). Clustering of membrane raft proteins by the actin cytoskeleton. *J. Biol. Chem.* **282**, 36682-36691.

Chichili, G. R., Westmuckett, A. D. and Rodgers, W. (2010). T cell signal regulation by the actin cytoskeleton. *J. Biol. Chem.* **285**, 14737-14746.

Clarke, M., Engel, U., Giorgione, J., Muller-Taubenberger, A., Prassler, J., Veltman, D. and Gerisch, G. (2010). Curvature recognition and force generation in phagocytosis. *BMC Biol.* **8**, 154.

Eitzen, G., Wang, L., Thorngren, N. and Wickner, W. (2002). Vacuole-bound actin regulates homotypic membrane fusion. *J. Cell Biol.* **158**, 669-679.

Fratti, R. A. and Wickner, W. (2007). Distinct targeting and fusion functions of the PX and SNARE domains of yeast vacuolar Vam7p. *J. Biol. Chem.* **282**, 13133-13138.

Fratti, R. A., Jun, Y., Merz, A. J., Margolis, N. and Wickner, W. (2004). Interdependent assembly of specific regulatory lipids and membrane fusion proteins into the vertex ring domain of docked vacuoles. *J. Cell Biol.* **167**, 1087-1098.

Fratti, R. A., Collins, K. M., Hickey, C. M. and Wickner, W. (2007). Stringent 3Q: 1R composition of the SNARE 0-layer can be bypassed for fusion by compensatory SNARE mutation or by lipid bilayer modification. *J. Biol. Chem.* **282**, 14861-14867.

Galletta, B. J., Mooren, O. L. and Cooper, J. A. (2010). Actin dynamics and endocytosis in yeast and mammals. *Curr. Opin. Biotechnol.* **21**, 604-610.

Giardini, P. A., Fletcher, D. A. and Theriot, J. A. (2003). Compression forces generated by actin comet tails on lipid vesicles. *Proc. Natl. Acad. Sci. USA* **100**, 6493-6498.

Gillooly, D. J., Morrow, I. C., Lindsay, M., Gould, R., Bryant, N. J., Gaullier, J. M., Parton, R. G. and Stenmark, H. (2000). Localization of phosphatidylinositol 3-phosphate in yeast and mammalian cells. *EMBO J.* **19**, 4577-4588.

Goode, B. L. (2002). Purification of yeast actin and actin-associated proteins. *Methods Enzymol.* **351**, 433-441.

Haas, A. and Wickner, W. (1996). Homotypic vacuole fusion requires Sec17p (yeast alpha-SNAP) and Sec18p (yeast NSF). *EMBO J.* **15**, 3296-3305.

Haas, A., Conradt, B. and Wickner, W. (1994). G-protein ligands inhibit in vitro reactions of vacuole inheritance. *J. Cell Biol.* **126**, 87-97.

Haas, A., Scheglmann, D., Lazar, T., Gallwitz, D. and Wickner, W. (1995). The GTPase Ypt7p of Saccharomyces cerevisiae is required on both partner vacuoles for the homotypic fusion step of vacuole inheritance. *EMBO J.* **14**, 5258-5270.

Hao, M. and Bogan, J. S. (2009). Cholesterol regulates glucose-stimulated insulin secretion through phosphatidylinositol 4,5-bisphosphate. *J. Biol. Chem.* **284**, 29489-29498.

Hartwig, J. H. and Yin, H. L. (1988). The organization and regulation of the macrophage actin skeleton. *Cell Motil. Cytoskeleton.* **10**, 117-125.

Isgandarova, S., Jones, L., Forsberg, D., Loncar, A., Dawson, J., Tedrick, K. and Eitzen, G. (2007). Stimulation of actin polymerization by vacuoles via Cdc42p-dependent signaling. *J. Biol. Chem.* **282**, 30466-30475.

Jahn, R. and Sudhof, T. C. (1999). Membrane fusion and exocytosis. *Annu. Rev. Biochem.* **68**, 863-911.

Johnson, J. E., Giorgione, J. and Newton, A. C. (2000). The C1 and C2 domains of protein kinase C are independent membrane targeting modules, with specificity for phosphatidylserine conferred by the C1 domain. *Biochemistry* **39**, 11360-11369.

Jun, Y., Fratti, R. A. and Wickner, W. (2004). Diacylglycerol and its formation by Phospholipase C regulate Rab- and SNARE-dependent yeast vacuole fusion. *J. Biol. Chem.* **279**, 53186-53195.

Jun, Y., Thorngren, N., Starai, V. J., Fratti, R. A., Collins, K. and Wickner, W. (2006). Reversible, cooperative reactions of yeast vacuole docking. *EMBO J.* **25**, 5260-5269.

Kwik, J., Boyle, S., Fooksman, D., Margolis, L., Sheetz, M. P. and Edidin, M. (2003). Membrane cholesterol, lateral mobility, and the phosphatidylinositol 4,5-bisphosphate-dependent organization of cell actin. *Proc. Natl. Acad. Sci. USA* **100**, 13964-13969.

Liebl, D. and Griffiths, G. (2009). Transient assembly of F-actin by phagosomes delays phagosome fusion with lysosomes in cargo-overloaded macrophages. *J. Cell Sci.* **122**, 2935-2945.

Marcus, S. L., Wenk, M. R., Steele-Mortimer, O. and Finlay, B. B. (2001). A synaptojanin-homologous region of Salmonella typhimurium SigD is essential for inositol phosphatase activity and Akt activation. *FEBS Lett.* **494**, 201-207.

Mayer, A. and Wickner, W. (1997). Docking of yeast vacuoles is catalyzed by the Ras-like GTPase Ypt7p after symmetric priming by Sec18p (NSF). *J. Cell Biol.* **136**, 307-317.

Mayer, A., Wickner, W. and Haas, A. (1996). Sec18p (NSF)-driven release of Sec17p (alpha-SNAP) can precede docking and fusion of yeast vacuoles. *Cell* **85**, 83-94.

Mayer, A., Scheglmann, D., Dove, S., Glatz, A., Wickner, W. and Haas, A. (2000). Phosphatidylinositol 4,5-bisphosphate regulates two steps of homotypic vacuole fusion. *Mol. Biol. Cell* **11**, 807-817.

Merz, A. J. and Wickner, W. T. (2004a). *Trans*-SNARE interactions elicit Ca^{2+} efflux from the yeast vacuole lumen. *J. Cell Biol.* **164**, 195-206.

Merz, A. J. and Wickner, W. T. (2004b). Resolution of organelle docking and fusion kinetics in a cell-free assay. *Proc. Natl. Acad. Sci. USA* **101**, 11548-11553.

Mogilner, A. and Keren, K. (2009). The shape of motile cells. *Curr. Biol.* **19**, R762-R771.

Morton, W. M., Ayscough, K. R. and McLaughlin, P. J. (2000). Latrunculin alters the actin-monomer subunit interface to prevent polymerization. *Nat. Cell Biol.* **2**, 376-378.

Nichols, B. J., Ungermann, C., Pelham, H. R., Wickner, W. T. and Haas, A. (1997). Homotypic vacuolar fusion mediated by t- and v-SNAREs. *Nature* **387**, 199-202.

Pollard, T. D. (2010). Mechanics of cytokinesis in eukaryotes. *Curr. Opin. Cell Biol.* **22**, 50-56.

Pollard, T. D. and Cooper, J. A. (2009). Actin, a central player in cell shape and movement. *Science.* **326**, 1208-1212.

Reese, C. and Mayer, A. (2005). Transition from hemifusion to pore opening is rate limiting for vacuole membrane fusion. *J. Cell Biol.* **171**, 981-990.

Reese, C., Heise, F. and Mayer, A. (2005). Trans-SNARE pairing can precede a hemifusion intermediate in intracellular membrane fusion. *Nature* **436**, 410-414.

Rohatgi, R., Ho, H. Y. and Kirschner, M. W. (2000). Mechanism of N-WASP activation by CDC42 and phosphatidylinositol 4,5-bisphosphate. *J. Cell Biol.* **150**, 1299-1310.

Rosenthal, J. A., Chen, H., Slepnev, V. I., Pellegrini, L., Salcini, A. E., Di Fiore, P. P. and De Camilli, P. (1999). The epsins define a family of proteins that interact with components of the clathrin coat and contain a new protein module. *J. Biol. Chem.* **274**, 33959-33965.

Rozelle, A. L., Machesky, L. M., Yamamoto, M., Driessens, M. H., Insall, R. H., Roth, M. G., Luby-Phelps, K., Marriott, G., Hall, A. and Yin, H. L. (2000). Phosphatidylinositol 4,5-bisphosphate induces actin-based movement of raft-enriched vesicles through WASP-Arp2/3. *Curr. Biol.* **10**, 311-320.

Seals, D. F., Eitzen, G., Margolis, N., Wickner, W. T. and Price, A. (2000). A Ypt/Rab effector complex containing the Sec1 homolog Vps33p is required for homotypic vacuole fusion. *Proc. Natl. Acad. Sci. USA* **97**, 9402-9407.

Sokal, R. R. and Rohlf, F. J. (1994). *Biometry: The Principles and Practice of Statistics in Biological Research.* pp. 859, W. H. Freeman.

Szymanska, E., Sobota, A., Czurylo, E. and Kwiatkowska, K. (2008). Expression of PI(4,5)P2-binding proteins lowers the PI(4,5)P2level and inhibits FcgammaRIIA-mediated cell spreading and phagocytosis. *Eur. J. Immunol.* **38**, 260-272.

Taylor, G. S., Maehama, T. and Dixon, J. E. (2000). Inaugural article: myotubularin, a protein tyrosine phosphatase mutated in myotubular myopathy, dephosphorylates the lipid second messenger, phosphatidylinositol 3-phosphate. *Proc. Natl. Acad. Sci. USA.* **97**, 8910-8915.

Tamkun, M. M., O'Connell, K. M. and Rolig, A. S. (2007). A cytoskeletal-based perimeter fence selectively corrals a sub-population of cell surface Kv2.1 channels. *J. Cell Sci.* **120**, 2413-2423.

Ungermann, C. and Wickner, W. (1998). Vam7p, a vacuolar SNAP-25 homolog, is required for SNARE complex integrity and vacuole docking and fusion. *EMBO J.* **17**, 3269-3276.

Ungermann, C., Sato, K. and Wickner, W. (1998). Defining the functions of trans-SNARE pairs. *Nature* **396**, 543-548.

Upadhyaya, A., Chabot, J. R., Andreeva, A., Samadani, A. and van Oudenaarden, A. (2003). Probing polymerization forces by using actin-propelled lipid vesicles. *Proc. Natl. Acad. Sci. USA* **100**, 4521-4526.

Vallance, B. A. and Finlay, B. B. (2000). Exploitation of host cells by enteropathogenic Escherichia coli. *Proc. Natl. Acad. Sci. USA* **97**, 8799-8806.

van Rheenen, J., Song, X., van Roosmalen, W., Cammer, M., Chen, X., Desmarais, V., Yip, S. C., Backer, J. M., Eddy, R. J. and Condeelis, J. S. (2007). EGF-induced PIP2 hydrolysis releases and activates cofilin locally in carcinoma cells. *J. Cell Biol.* **179**, 1247-1259.

Wang, L., Ungermann, C. and Wickner, W. (2000). The docking of primed vacuoles can be reversibly arrested by excess Sec17p (alpha-SNAP). *J. Biol. Chem.* **275**, 22862-22867.

Wang, L., Seeley, E. S., Wickner, W. and Merz, A. J. (2002). Vacuole fusion at a ring of vertex docking sites leaves membrane fragments within the organelle. *Cell* **108**, 357-369.

Wang, L., Merz, A. J., Collins, K. M. and Wickner, W. (2003). Hierarchy of protein assembly at the vertex ring domain for yeast vacuole docking and fusion. *J. Cell Biol.* **160**, 365-374.

Wickner, W. (2010). Membrane fusion: five lipids, four SNAREs, three chaperones, two nucleotides, and a Rab, all dancing in a ring on yeast vacuoles. *Annu. Rev. Cell Dev. Biol.* **26**, 115-136.

Wiradjaja, F., Ooms, L. M., Tahirovic, S., Kuhne, E., Devenish, R. J., Munn, A. L., Piper, R. C., Mayinger, P. and Mitchell, C. A. (2007). Inactivation of the phosphoinositide phosphatases Sac1p and Inp54p leads to accumulation of phosphatidylinositol 4,5-bisphosphate on vacuole membranes and vacuolar fusion defects. *J. Biol. Chem.* **282**, 16295-16307.